Controls on mangrove forest-atmosphere carbon dioxide exchanges in western Everglades National Park

Jordan G. Barr,[1] Vic Engel,[1] José D. Fuentes,[2] Joseph C. Zieman,[3] Thomas L. O'Halloran,[4] Thomas J. Smith III,[5] and Gordon H. Anderson[6]

Received 9 November 2009; revised 16 February 2010; accepted 12 March 2010; published 17 June 2010.

[1] We report on net ecosystem production (NEP) and key environmental controls on net ecosystem exchange (NEE) of carbon dioxide (CO_2) between a mangrove forest and the atmosphere in the coastal Florida Everglades. An eddy covariance system deployed above the canopy was used to determine NEE during January 2004 through August 2005. Maximum daytime NEE ranged from −20 to −25 μmol (CO_2) m^{-2} s^{-1} between March and May. Respiration (R_d) was highly variable (2.81 ± 2.41 μmol (CO_2) m^{-2} s^{-1}), reaching peak values during the summer wet season. During the winter dry season, forest CO_2 assimilation increased with the proportion of diffuse solar irradiance in response to greater radiative transfer in the forest canopy. Surface water salinity and tidal activity were also important controls on NEE. Daily light use efficiency was reduced at high (>34 parts per thousand (ppt)) compared to low (<17 ppt) salinity by 46%. Tidal inundation lowered daytime R_d by ~0.9 μmol (CO_2) m^{-2} s^{-1} and nighttime R_d by ~0.5 μmol (CO_2) m^{-2} s^{-1}. The forest was a sink for atmospheric CO_2, with an annual NEP of 1170 ± 127 g C m^{-2} during 2004. This unusually high NEP was attributed to year-round productivity and low ecosystem respiration which reached a maximum of only 3 g C m^{-2} d^{-1}. Tidal export of dissolved inorganic carbon derived from belowground respiration likely lowered the estimates of mangrove forest respiration. These results suggest that carbon balance in mangrove coastal systems will change in response to variable salinity and inundation patterns, possibly resulting from secular sea level rise and climate change.

Citation: Barr, J. G., V. Engel, J. D. Fuentes, J. C. Zieman, T. L. O'Halloran, T. J. Smith III, and G. H. Anderson (2010), Controls on mangrove forest-atmosphere carbon dioxide exchanges in western Everglades National Park, *J. Geophys. Res.*, *115*, G02020, doi:10.1029/2009JG001186.

1. Introduction

[2] Despite the extensive ongoing carbon sequestration research using carbon dioxide (CO_2) eddy covariance (EC) flux towers [*Baldocchi et al.*, 2001; *Baldocchi*, 2008], little information exists on the carbon assimilation capacity of ecosystems situated along the marine-terrestrial interface [*Wofsy and Harris*, 2002]. Mangrove forests represent important ecosystems to investigate because of their pantropical distribution [*Chapman*, 1976; *Tomlinson*, 1986], rich biogeochemistry [*Robertson and Alongi*, 1992; *Twilley et al.*, 1992], and high rates of productivity [*Mitsch and Gosselink*, 2000; *Smith et al.*, 1994; *Ward et al.*, 2006], estimated at 218 ± 72 Tg C yr^{-1} globally [*Bouillon et al.*, 2008].

[3] The carbon balance of a mangrove forest is modulated by the climatic and environmental factors that regulate terrestrial forests, such as temperature, solar irradiance, and nutrient levels, and by others such as tidal activity and salinity unique to coastal habitats. Midday photosynthetic rates in *Rhizophora mangle* (red mangroves) tend to decline at high leaf temperatures (>303 K) coincident with stomatal closure at high (>2 kPa) vapor pressure deficit (VPD) and high (>1000 μmol (photons) m^{-2} s^{-1}) photosynthetic active radiation (PAR) [*Cheeseman and Lovelock*, 2004; *Barr*, 2005]. However, in the tropics and subtropics where mangroves are found, the development of afternoon thunderstorms and overcast conditions can also result in PAR-limited carbon assimilation [*Barr et al.*, 2009]. Soil nutrients are known to limit growth in many mangrove forests [*Koch*, 1997; *Lovelock et al.*, 2004, 2006; *Krauss et al.*, 2006;

[1]South Florida Natural Resource Center, Everglades National Park, Homestead, Florida, USA.
[2]Department of Meteorology, Pennsylvania State University, University Park, Pennsylvania, USA.
[3]Department of Environmental Sciences, University of Virginia, Charlottesville, Virginia, USA.
[4]Department of Forest Ecosystems and Society, Oregon State University, Corvallis, Oregon, USA.
[5]Florida Integrated Science Center, U.S. Geological Survey, St. Petersburg, Florida, USA.
[6]Everglades National Park Field Station, Florida Integrated Science Center, U.S. Geological Survey, Homestead, Florida, USA.

0148-0227/10/2009JG001186

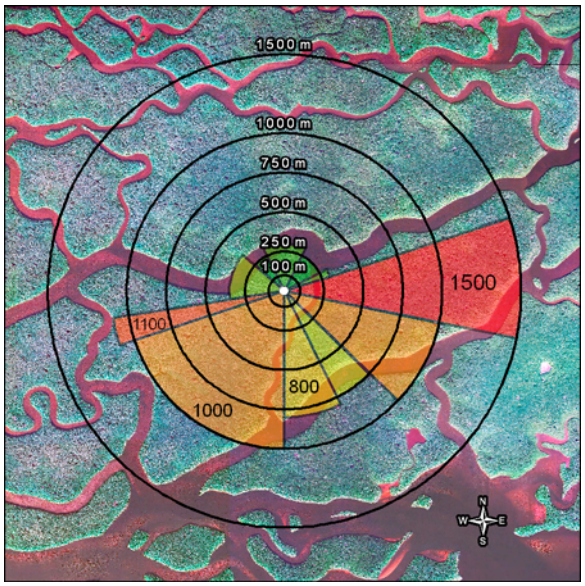

Figure 1. Aerial photograph of the study site including a visualization of available fetch from all wind directions. NEE values were determined to be valid if >50% of the cumulative flux originated within the fetch boundaries contained by the tidal channels bordering the site.

Feller et al., 2003]. Duration of tidal inundation is another important factor regulating mangrove productivity directly [e.g., *Naidoo et al.*, 1997] or indirectly through its effect on nutrient availability [*Krauss et al.*, 2006]. Salinity can be an important driver regulating photosynthesis and stomatal conductance in mangroves [*Ball and Farquhar*, 1984; *Clough and Sim*, 1989; *Ball and Pidsley*, 1995; *Takemura et al.*, 2000; *Parida et al.*, 2004; *Lopez-Hoffman et al.*, 2006]. The carbon balance in mangrove forests is thus partially influenced by the physical conditions that regulate salinity in coastal environments, including interannual variability in rainfall and freshwater discharge.

[4] The long-term survival of many mangrove forests depends on sediment surface elevations keeping pace with relative sea level rise [*Whelan et al.*, 2005; *Krauss et al.*, 2003]. Relative rates of net primary production versus respiration and peat decomposition may well determine the survival of many forests, with mangroves in some regions facing collapse given current and projected future rates of sea level rise [*Alongi*, 2008]. Carbon budget approaches such as those cited by *Bouillon et al.* [2008] provide insights into carbon sources and sinks in mangrove ecosystems in relation to coastal habitat qualities. On the other hand, EC measurements allow investigation of the environmental controls on net primary productivity and respiration and how these processes respond to local climatic variables, tidal activity, and salinity levels on subdaily time scales. This paper contributes to this goal by using estimates of net ecosystem exchange (NEE) of atmospheric CO_2 between a mature mangrove forest and atmosphere in the western Florida Everglades. NEE values were coupled with detailed measurements of meteorological variables, tidal cycles, and soil surface water salinity to investigate the processes controlling atmospheric CO_2 exchange. Our objectives in this study are (1) to identify the key environmental controls on canopy level CO_2 fluxes, (2) to establish the functional relationships between these controls and carbon assimilation and respiration rates, and (3) to quantify net annual ecosystem production (NEP) for a mature forest.

2. Research Methods

2.1. Site Description and Measurements

[5] The study site (25.3646°N, 81.0779°W) is located within an extensive riverine and fringing mangrove forest close to the mouth of the Shark River in western Everglades National Park (Figure 1). The dominant tree species at the site are red (*R. mangle*), black (*A. germinans*), and white (*L. racemosa*) mangroves reaching heights of 15–20 m [*Ewe et al.*, 2006]. The forest understory is sparse and composed of seedlings and juvenile mangroves with an average height less than 4 m. The region experiences semidiurnal tides and is inundated twice during most 24 h periods. High tides can reach up to 0.5 m above the sediment surface [*Krauss et al.*, 2006]. However, the sediment surface can be exposed for several days at a time during the annual minima in the solar tidal cycle which corresponds to the periods of low discharge through Shark River, generally in February, March, and April. The sediment surface at the site is ~0.2 m above mean sea level. Peat thickness beneath the forest increases toward the Gulf of Mexico in this region and at our site reaches 5 to 6 m [*Spackman et al.*, 1966].

[6] Approximately 60% of the annual rainfall in the Everglades falls during the May–October wet season [*Duever et al.*, 1994]. Seasonal rainfall patterns (Figure 2) are strongly influenced by the passage of tropical cyclones, usually between June and October, and by the infrequent passage of cold fronts during the winter months. With the onset of the wet season, total daily irradiance (Figure 3a) becomes variable due to frequent afternoon convective thunderstorms. Minimum daytime air temperatures (T_A) in the Everglades rarely fall below 10°C between December

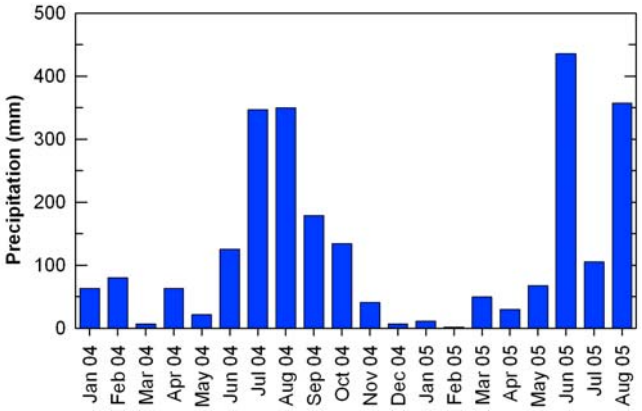

Figure 2. Monthly rainfall totals during January 2004 through August 2005. Values represent the average of rainfall totals from the Gulf Coast (GI) Everglades National Park station and the Shark Slough (SH2) United States Geological Survey station. Stations GI and SH2 are 5 km and 13 km E-NE of the study site.

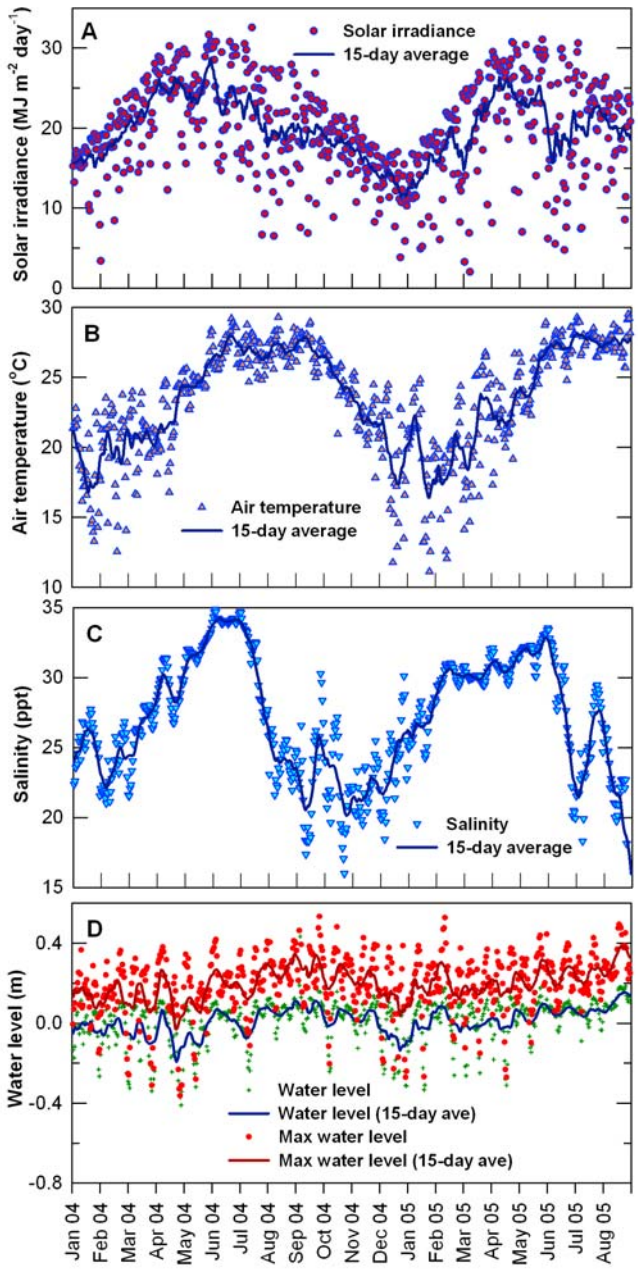

Figure 3. (a) Incident solar irradiance, (b) average daily (24 h) air temperature measured at 27 m above the ground, (c) average daily surface water salinity, and (d) average and maximum daily water level during January 2004 through August 2005. The 15 day centered moving averages of all daily values are included.

and February (Figure 3b). From March through November, the daily maximum T_A in the region is generally above 27°C [*Duever et al.*, 1994]. During 2004–2005, the minimum daytime T_A ranged from 10 to 15°C during the winter dry season, while the May–October wet season values were consistently above 25°C and less variable (Figure 3b). Soil surface water salinity at the site varies with tidal cycles and rainfall patterns. On daily time scales, salinity values increase from 1 to 12 ppt with incoming tides (Figure 3c). However, the annual minimum salinity values (2–18 ppt) during 2000–2010 occur when water levels are at their highest during the peak of the annual tidal cycle and freshwater discharges. Salinity values are highest (30–35 ppt) at the end of the dry season in May and early June. Annual minimum water levels occur during the early dry season in February and March when troughs in the lunar monthly tidal component combine with minimal fresh water flow through Shark River. Water levels are relatively high (>0.3 m) during this period (Figure 3d) due to increased fresh water discharge into Shark River. The peak of the annual tidal cycle also occurs during the wet season [*Stumpf and Haines*, 1998].

[7] A 30 m flux tower and 250 m boardwalk from the banks of Shark River were constructed in June 2003. The tower base is 1.5 m above the surface and is supported by a square grid of central tiers (9 cm by 9 cm by 3.7 m long) driven 3 m into the sediment. Crossbeams to peripheral tiers provide additional stability and prevent the structure from sinking into the peat. Guy wires are anchored on smaller platforms with similar tiered construction. An elevated and waterproof wooden hut at the tower base houses twelve 6 V (260 A hr each) rechargeable batteries. All electronics are housed in a waterproof box elevated 2 m above the sediment. Five 120 W solar panels maintain battery charge. The tower (Universal Manufacturing, Clinton Twp., Michigan) is composed of 22″ wide by 10′ tall triangular aluminum sections. From the tower site, specific and uniform fetch distances (Figure 1) are determined from river boundaries and are as follows (where 0° is N, increasing in the clockwise direction): 300 m from 0° to 70°, 1500 m from 70° to 120°, 1000 m from 120° to 135°, 800 m from 135° to 180°, 1300 m from 180° to 270°, 250 m to 300 m from 270° to 360°.

[8] Environmental variables were measured above the canopy at 1 s intervals, averaged over 30 min on two data loggers (model CR23X, Campbell Scientific, Logan, Utah), and uploaded to a laptop for storage. These measurements include net radiation (model CNR 1, Kipp and Zonen, Bohemia, New York) and incoming and reflected PAR (model LI-190SB, LI-COR, Inc., Lincoln, Nebraska). Measurements also include air temperature (T_A) and humidity (model HMP45C, Campbell Scientific, Inc., Logan, Utah) and wind speed and direction (model 05103 RM Young, Traverse City, Michigan) measured at 27 m. Aspirated and shielded thermometers (model 107 temperature probes, Campbell Scientific, Inc.) measure air temperature at 20 m, 15 m, 11 m, 6 m, and 1.5 m above the ground. Heat flux plates (model HFT 3.1, Campbell Scientific, Inc.) record soil heat fluxes, and soil thermocouples (model 105T, Campbell Scientific, Inc.) measure soil temperature (T_s) at −5 cm, −10 cm, −20 cm, and −50 cm. Further details on tower measurements are provided by *Barr* [2005]. Hydrologic data were continuously monitored and recorded every 15 min at a station 30 m south of Shark River and 150 m west of the flux tower. Measurements included specific conductivity and temperature (model 600R water quality sampling sonde, YSI Inc., Yellow Springs, Ohio) of surface well water and water level (model Waterlog H-333 shaft encoder, Design Analysis Associates, Logan, Utah).

[9] The eddy covariance (EC) system is mounted at 27 m. The EC consists of a three-dimensional sonic anemometer

Table 1. Summary of Annual NEP and Errors Associated With the Gap-Filling Technique

Parameter	Average ± Standard Deviation
Bias error, BE (μmol CO_2 m^{-2} s^{-1})	−0.021 ± 0.054
RMSE (μmol CO_2 m^{-2} s^{-1})	3.56 ± 0.058
NEP_{2004} (g C m^{-2} $year^{-1}$)	1170 ± 127
NEP^a_{2005} (g C m^{-2} $year^{-1}$)	832 ± 97

[a]Through the end of August 2005.

(model RS-50, Gill Co., Lymington, England) and thermistor and an open path infrared CO_2 and water vapor (H_2O) gas analyzer (model LI-7500, LI-COR, Inc., Lincoln, Nebraska). High-frequency (10 Hz) measurements are stored and processed with custom software to derive half-hourly CO_2, latent and sensible heat, and momentum exchanges between the forest and the overlying atmosphere. High-frequency data processing consists of spike removal [*Vickers and Mahrt*, 1997], a two-dimensional coordinate rotation of the wind field, a time lag correction of CO_2 concentration to maximize covariance with vertical wind speed variation, buoyancy corrections of sonic air temperatures [*Schotanus et al.*, 1983], and conversion of the turbulent flux into the total constituent flux [*Webb et al.*, 1980], which accounts for the positive vertical mass flow resulting from positive buoyancy of less dense air parcels. Storage of CO_2 in the air column below the EC system was estimated based on the half-hourly rate of change of CO_2 concentrations at the infrared analyzer level [*Morgenstern et al.*, 2004; *Humphreys et al.*, 2005]. This storage term was added to the fluxes derived from the EC system to determine NEE. The algorithms used to calculate NEE were independently verified using AmeriFlux "gold file" data sets (http://public.ornl.gov/ameriflux/standards-gold.shtml).

2.2. Missing Data

[10] Missing or invalid EC fluxes are commonly referred to as "gaps." Gaps occur when gas concentrations are out of range (as occurs during precipitation events), when turbulence is weak or intermittent, or when there is insufficient fetch. The CO_2 fluxes during these gap periods need to be included to determine annual NEE cycles [*Falge et al.*, 2001]. At the study site, short-duration gaps (≤4.5 h) occurred primarily at night but also happened as the result of thunderstorms and breaks in the power supply. Nighttime flux data were discarded during periods of weak turbulence [*Goulden et al.*, 1996; *Lee et al.*, 1999] when the friction velocity (u*) was less than 0.21 m s^{-1}. This u* threshold was calculated by first dividing nighttime NEE values into 20 u* classes for each bimonthly period and then defining a u* value above which NEE became invariant or, for those bimonthly periods where no clear relationship between NEE and u* was apparent, we chose a u* value which corresponded to an NEE value ≥85% of the maximum bimonthly NEE. The global u* threshold of 0.21 m s^{-1} applied in the data analysis is the median value of all bimonthly u* threshold values, which varied between 0.15 m s^{-1} and 0.30 m s^{-1}. During three bimonthly periods, the u* threshold was >0.25 m s^{-1}. However, the differences in fluxes calculated during these periods using a u* threshold of 0.21 m s^{-1} versus greater values up to 0.3 m s^{-1} were not significant. Therefore, the global u* threshold of 0.21 m s^{-1} was applied to all bimonthly periods.

[11] Flux data were discarded when the flux footprint [*Schuepp et al.*, 1990; *Schmid*, 2002] extended beyond the forest fetch. The fetch exceeded the footprint most frequently (66% of the time) during the nighttime when winds originated from the NW to NE. Longer gaps (>4.5 h) in the data set were generally caused by instrument or data acquisition malfunction and on rare occasions lasted for several days. The combined duration of gaps comprised 61%, 28%, and 46% of the total nighttime, daytime, and combined data sets, respectively. These values are comparable to average nighttime gap duration of 65% reported for 10 forested sites in Europe [*Moffat et al.*, 2007].

2.3. Gap Filling and Error Analysis

[12] Several strategies are available to gap fill eddy covariance CO_2 fluxes [see *Moffat et al.*, 2007; *Gu et al.*, 2005; *Falge et al.*, 2001]. We chose a mean diurnal variation (MDV) method to fill short gaps and look-up tables (LUT) for longer gaps. The MDV utilizes a 14 day moving window centered on the day of the gap, and the missing values are filled with the mean fluxes within this window occurring during the same half-hourly period as the gap. For longer gaps, separate daytime and nighttime LUTs were developed for each 2 month interval beginning on 1 January 2004. Nighttime T_A was better correlated with CO_2 fluxes than T_S and was therefore chosen as the independent variable in the LUT. For each 2 month interval, half-hourly nighttime CO_2 fluxes were partitioned into 20 T_A bins, each containing the same number of values. For daytime half-hourly CO_2 fluxes, a two-dimensional LUT was constructed using 16-PAR and 3-T_A bin categories. *Falge et al.* [2001] provide additional details on appropriate LUT dimensions when gap-filling EC fluxes.

[13] Potential error and bias in the fluxes, introduced by the MDV and the LUT, were estimated by randomly creating and then refilling a set of artificial gaps [*Moffat et al.*, 2007] overlapping with valid data periods. On a monthly basis, the sum of the artificial daytime and the nighttime gaps were constructed to have the same duration as actual gaps. The root-mean-square error (RMSE) and the bias error (BE) were determined by comparing the fluxes estimated from 100 simulations of randomly generated, then filled, artificial gaps to the concurrent valid observations (Table 1). Small BE values (−0.021 ± 0.054 μmol (CO_2) m^{-2} s^{-1}) suggest this method imputed minimal bias in annual NEP estimates. The RMSE (3.56 ± 0.058 μmol (CO_2) m^{-2} s^{-1}) was within the range of those reported for six forested sites in Europe [*Moffat et al.*, 2007].

[14] Confidence intervals on monthly NEP were computed using the results of the gap filling procedure. In this method, all of the half-hourly NEE values for each month, including valid and gap-filled data, were integrated to give an estimate of monthly NEP for each of the 100 gap-filling simulations. The 5th and 95th percentiles of monthly NEP for each month were derived from the results. The average percent relative error (RE) was then calculated as the difference between the 95th and the 5th percentiles of gap-filled NEP divided by 2. In some cases, particularly during summer nighttime periods, the duration of actual gaps represented more than 50% of the total duration of nighttime

periods within a 1 month interval. For these months, the amount of valid data points was considered insufficient to accurately calculate the RE associated with the gap-filling procedure. To account for this, a relationship between RE and the percentage of artificial gaps was derived by imposing a range of artificial gap fractions up to 80% of the valid data periods for those months with actual gaps <10%. A power function was then fit to the complete set of RE values associated with the fraction of data gaps (f_{gap}) for each month using least squares regression:

$$RE = 7.66\, f_{gap}^{0.366}. \quad (1)$$

Monthly NEP confidence intervals were calculated as the product of NEP values derived from valid data points and RE based on the fraction of gaps (f_{gap}) in that month using (1).

2.4. Light and Temperature Responses

[15] Daytime NEE responses to PAR were determined separately for "high" (T_A > 28°C) and "low" air temperatures (T_A < 21°C). High and low air temperature included 16.2% and 21.3% of the daytime flux data set, respectively. Daytime NEE values were further grouped by a clearness index (K_t), defined as S/S_e, where S is incoming solar irradiance (W m^{-2}) and S_e is extraterrestrial irradiance at the top of the atmosphere on a plane parallel to the Earth's surface:

$$S_e = S_{sc}(1 + 0.033\ \cos(360\ t_d/365))\cos\ \theta. \quad (2)$$

S_{sc} is the solar constant (1370 W m^{-2}), t_d is day of year, and Θ is the solar zenith angle [*Spitters et al.*, 1986; *Gu et al.*, 2002]. Lower ($K_t \leq 0.65$) and higher ($K_t > 0.65$) values of K_t represent cloudy skies and clear skies, respectively. The threshold value of K_t (0.65) was selected as the median of daytime values during the study period. Daytime NEE values were distributed evenly into cloudy and clear sky bin categories across the high and low temperature ranges. To reduce the scatter and variability of half-hourly NEE versus PAR, NEE values were bin averaged across 30 intervals of PAR. A form of the Michaelis-Menten equation (3) was fit to the bin-averaged NEE data using nonlinear least squares regression:

$$NEE = -\frac{a'\ PAR}{(1 - (\mathrm{PAR}/2000) + (a'\ PAR/GEP_{2000}))} + R_d. \quad (3)$$

The variable a′ represents the ecosystem quantum yield (μmol (CO_2) per (μmol (photons)). GEP_{2000} is the gross ecosystem photosynthesis (μmol (CO_2) m^{-2} s^{-1}) defined as the sum of daytime NEE and the ecosystem respiration rate R_d (μmol (CO_2) m^{-2} s^{-1}) when PAR equals 2000 μmol (photons) m^{-2} s^{-1}.

2.5. Salinity Effects

[16] Direct salinity effects on NEE in mangroves are difficult to quantify because both short- and long-term fluctuations in salinity are also typically accompanied by changes in tidal cycles, temperature, and solar irradiance, all of which influence canopy-scale CO_2 fluxes. We examined the potential effects of salinity on ecosystem functioning by comparing the relationships between daytime NEE, PAR, and T_A at salinity values above and below the daytime annual median of 29 ppt. PAR and daytime T_A data were divided into 20 and 15 bins, respectively, for each period characterized by "high" (>29 ppt) or "low" (≤29 ppt) salinity. Bin ranges were selected such that NEE values were equally distributed along PAR and T_A dimensions. Contours of equal NEE values were then constructed across the two dimensions of the PAR-T_A matrix (Sigma Plot Version 11, Systat Software, Inc., San Jose, California). We also investigated salinity effects on GEP [*Lopez-Hoffman et al.*, 2006; *Theuri et al.*, 1999; *Ball and Pidsley*, 1995; *Suárez and Medina*, 2006]. Daily total GEP was normalized by daily total PAR (here termed the light use efficiency (LUE)). We investigated the covariance between LUE and daily average salinity at PAR > 600 μmol (photons) m^{-2} s^{-1}:

$$LUE = \frac{\sum_{PAR>600} GEP}{\sum_{PAR>600} PAR}. \quad (4)$$

2.6. Ecosystem Respiration and Tidal Effects

[17] Equation (3) was used to estimate average daytime plant and soil respiration rates separately during high and low tides. In this method, a moving 7 day window of half-hourly PAR and NEE data was centered on each day in the record. Nonlinear regression was used to calculate daily R_d separately for high- (water level > 0.2 m) and low-tide (water level ≤ 0.2 m) periods. At least 30 valid NEE values were required within each tidal cycle during the 7 day window to calculate a high- and low-tide R_d for each day. An Arrhenius-type relationship [*Lloyd and Taylor*, 1994] was used to model daytime R_d as a function of air temperature:

$$R_d = R_{d20}\ \exp\left[\frac{E_a}{R}(1/293K - 1/T_K)\right]. \quad (5)$$

$R_{d_{20}}$ (μmol (CO_2) m^{-2} s^{-1}) is the ecosystem respiration rate at 20°C, E_a (in J mol^{-1}) is the apparent activation energy, R is the universal ideal gas constant (J mol^{-1} K^{-1}), and T_K is the average absolute air temperature during the 7 day moving window. The base respiration rate at 20°C was included rather than the more commonly used 10°C since daytime temperature values of 10°C are rare at the study site. Half-hourly GEP values were calculated as the sum of −NEE and R_d, with the results assigned to either the high- or the low-tide category. High- and low-tide GEP values were summed and used to determine daily LUE in (4). Nighttime R_d was modeled as a function of temperature using (5) for high- and low-tide periods. Three or more consecutive half-hourly R_d values within each tidal cycle were required for inclusion in the analysis.

2.7. Seasonal and Annual NEP

[18] Half-hourly, gap-filled NEE values were converted to carbon equivalents and summed over 24 h periods to produce daily total net ecosystem production NEP (g C m^{-2} d^{-1}). Daytime and nighttime components of NEP were calculated separately. Monthly sums of daily NEP illustrate seasonal changes in mangrove carbon assimilation in relation to

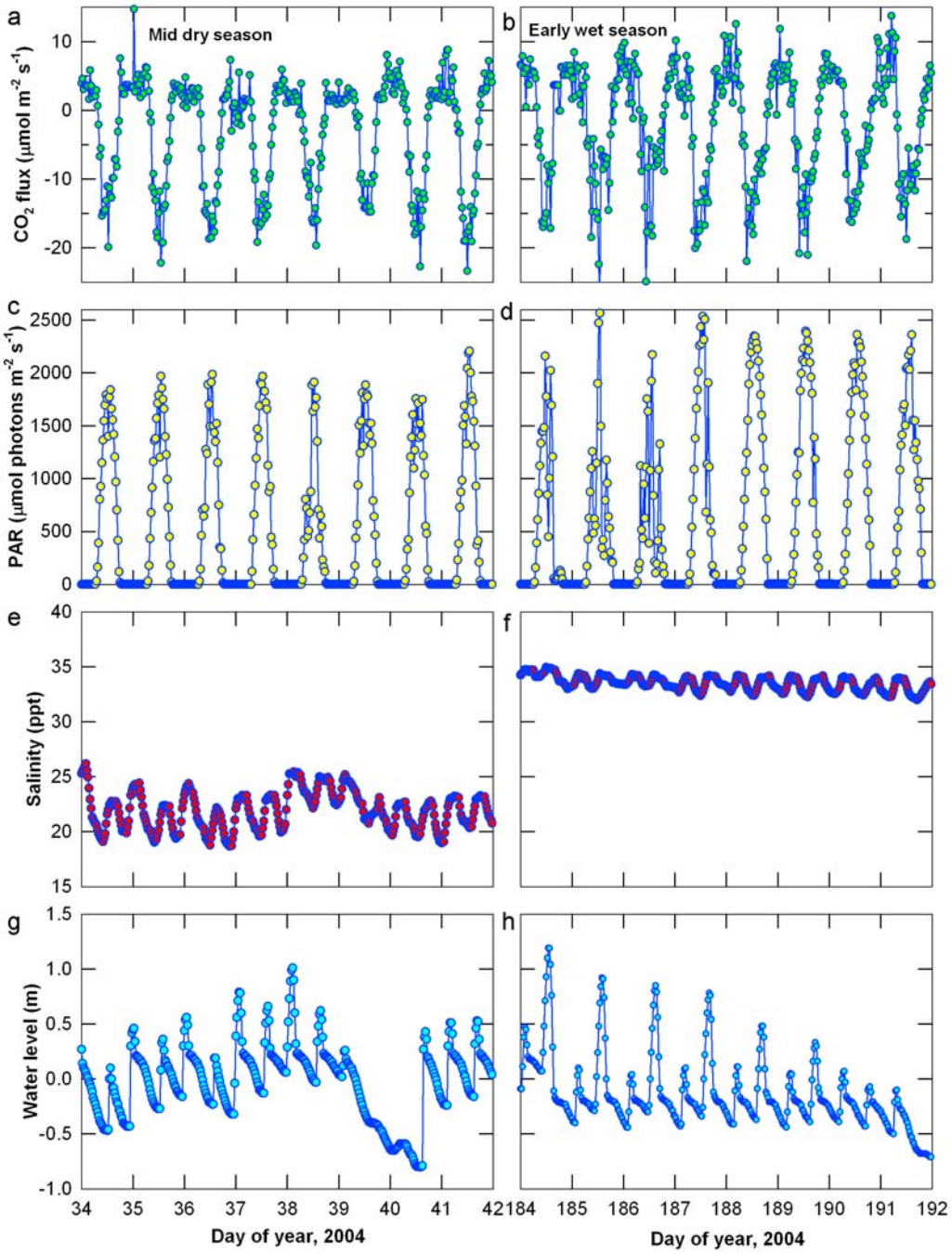

Figure 4. Representative diurnal CO_2 flux patterns during the (a) mid-dry season and (b) mid-wet season. (c and d) Photosynthetic active irradiance levels, (e and f) surface water salinity, and (g and h) water level are included for the same dry season (Figures 4c, 4e, and 4g) and wet season (Figures 4d , 4f, and 4h) periods as the CO_2 fluxes.

climatic and physical drivers such as salinity and water levels.

3. Results

3.1. Seasonal Factors Controlling NEE

[19] Throughout 2004–2005, NEE exhibited variable patterns primarily in response to differences in T_A (Figure 3b) and PAR (Figure 4). Midday, dry season NEE in 2004–2005 ranged from −15 to −25 μmol (CO_2) m^{-2} s^{-1}, while nighttime R_d during this period was generally <5 μmol (CO_2) m^{-2} s^{-1} and seldom exceeded 8 μmol (CO_2) m^{-2} s^{-1}. NEE generally decreased with T_A in February and March while salinity values remained low (18-28 ppt). With the onset of the wet season and higher T_A (>25°C), nighttime R_d increased up to 10 μmol (CO_2) m^{-2} s^{-1}, and daytime NEE increased to −14 to −23 μmol (CO_2) m^{-2} s^{-1}. Minimum daily NEE was as high as −5 μmol (CO_2) m^{-2} s^{-1} when

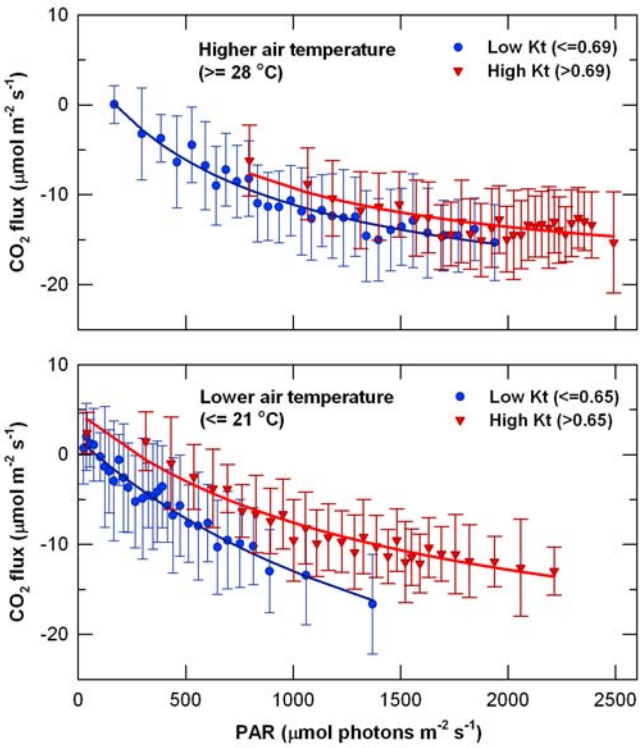

Figure 5. Half-hourly CO_2 flux response to PAR for the (top) highest (≥28°C) air temperatures and (bottom) lowest (≤21°C) air temperatures during January 2004 through August 2005 period when air temperature was measured at 27 m above ground. The CO_2 fluxes in each clearness index (K_t) range (Table 2) were bin averaged by PAR into 30 bins. The Michaelis-Menten function (3) was best fit to each set of binned values.

PAR dropped below ~800 μmol (photons) m^{-2} s^{-1} during this period as the result of afternoon convective cloud formation. During cloudless days, the lowest NEE values (−15 to −22 μmol (CO_2) m^{-2} s^{-1}) occurred during the late morning, 1–2 h and 3–4 h before the daily maximum in PAR and T_A, respectively. In general, NEE increased throughout the middle of the afternoon in the summer-wet season as T_A increased above 30°C. These patterns in R_d and midday NEE persisted until October when the frequency of thunderstorms decreased, daily solar irradiance (Figure 3a) became less variable, and the daily maximum T_A was <30°C.

3.2. NEE Responses to Light and Temperature

[20] NEE response to the proportion of diffuse irradiance (K_t) depended on air temperature (Figure 5). Temperature also affected the initial canopy quantum yield (a′) and daytime R_d, both of which were higher at $T_A \geq 28$°C compared to the values at $T_A \leq 21$°C (Table 2). This effect was apparent under both clear and cloudy sky conditions. At $T_A \leq 21$°C diffuse PAR conditions ($K_t \leq 0.69$) lead to a significant increase in GEP_{2000} ($p < 0.02$, one-tailed t test) and a decrease in R_d ($p < 0.01$, one-tailed t test), resulting in an average decrease of ~3 to 5 μmol (CO_2) m^{-2} s^{-1} in NEE.

[21] Minimum NEE values (−15 to −19 μmol (CO_2) m^{-2} s^{-1}) occurred when PAR varied between 1400 to 2100 μmol (photons) m^{-2} s^{-1} and T_A ranged from 24 to 28°C. NEE was higher at $T_A < 21$°C compared to rates at higher (>21°C) T_A and equivalent PAR. NEE was also generally 1–3 μmol (CO_2) m^{-2} s^{-1} higher when salinity values exceeded 29 ppt, PAR > 600 μmol m^{-2} s^{-1}, and 18°C < T_A < 33°C (Figure 6).

[22] There were small but significant linear decreases in LUE with increasing salinity (Figure 7). The slope of this relationship with 95% confidence intervals is −0.00042 ± −0.00008 μmol (CO_2) μmol (photons)$^{-1}$ ppt (salt)$^{-1}$ and is significantly different from zero ($p < 0.05$, one-tailed t test). A 48% decrease in LUE occurred when salinity levels increased from 16.7 to 34.7 ppt during the study period.

3.3. Ecosystem Respiration and Tidal Effects

[23] Daytime and nighttime R_d increased during low tides (Figure 8). The daytime reference respiration rate in the Arrhenius model, $R_{d,20}$, increased by 1.9 μmol (CO_2) m^{-2} s^{-1} during low-tide conditions ($p < 0.10$, one-tailed t test; Table 3). Daytime activation energies (E_a) in the model were also different ($p < 0.10$, one-tailed t test) between tidal cycles. Differences in R_d due to tides were greater during the daytime (0.9 μmol m^{-2} s^{-1}) compared to nighttime (0.5 μmol m^{-2} s^{-1}). High- and low-tide R_d converged at air temperatures above 29.5°C and 25.4°C during daytime and nighttime periods, respectively. Annual maxima nighttime R_d occurred during June through October reaching 4–7 μmol (CO_2) m^{-2} s^{-1}. Annual minimum nighttime R_d (1–3 μmol (CO_2) m^{-2} s^{-1}) occurred during December through February.

Table 2. Michaelis-Menton Parameters of Light Response During January 2004 though August 2005 for the Highest and Lowest Daytime Air Temperatures[a]

Panel	$T_{A,min}$	$T_{A,max}$	$K_{t,min}$	$K_{t,max}$	a′	GEP_{2000}	R_d	n
Highest temperatures	28.0	33.15	0.04	0.69	0.0376 ± 0.0126	20.93 ± 2.09	5.29 ± 2.27	1462
	28.0	33.15	0.69	1.00	0.0590 ± 0.0503	24.67 ± 9.41	11.11 ± 9.40	1462
p value[b]					0.503	0.523	0.327	
Lowest temperatures	5.5	21.0	0.02	0.65	0.0221 ± 0.0054	22.07 ± 2.41	1.74 ± 0.90	895
	5.5	21.0	0.65	1.00	0.0207 ± 0.0053	17.58 ± 1.34	4.78 ± 1.37	895
p value[b]					0.801	0.019	0.007	

[a]Highest daytime air temperatures are ≥28°C, and lowest daytime air temperatures are ≤21°C. For each temperature range, data were binned to represent high or low K_t. Higher and lower values of K_t represent clear and cloudy sky conditions, respectively. Significance tests were determined at the 95% confidence level. In the following form of the Michaelis-Menten equation, $NEE = a'PAR/(1-(PAR/2000) + (a'PAR/GEP_{2000}))-R_d$, NEE is the net ecosystem exchange of CO_2, a′ is the ecosystem quantum yield (μmol CO_2 (μmol PAR)$^{-1}$), GEP_{2000} is the gross ecosystem productivity (μmol CO_2 m^{-2} s^{-1}) at PAR = 2000 μmol m^{-2} s^{-1}, and R_d is the ecosystem respiration.

[b]The p values refer to the differences in Michaelis-Menten model parameters at high versus low K_t within a temperature range.

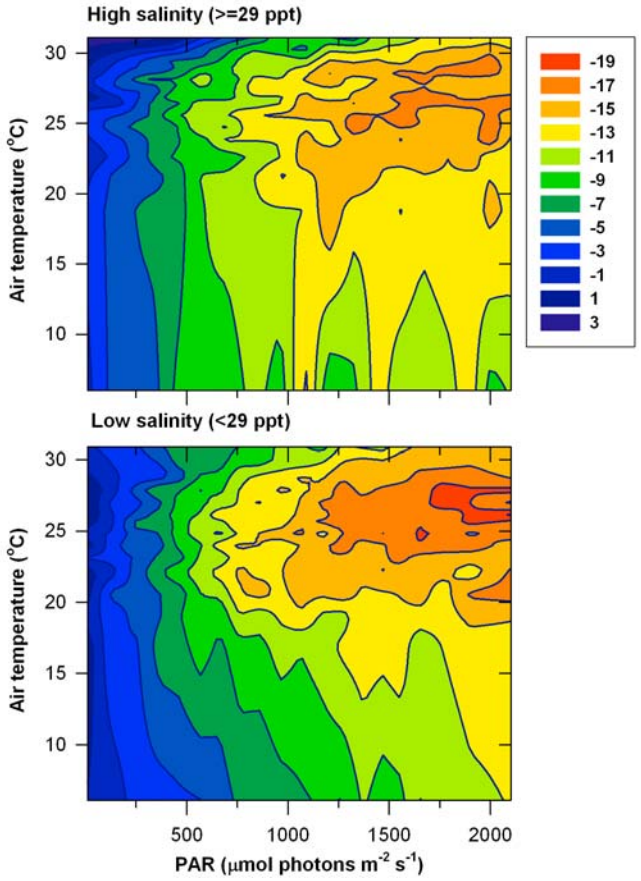

Figure 6. Contours of daytime average CO_2 flux as a function of both incident PAR and air temperature measured at 27 m above ground during both (top) high-salinity (≥29 ppt) and (bottom) low-salinity (<29 ppt) conditions.

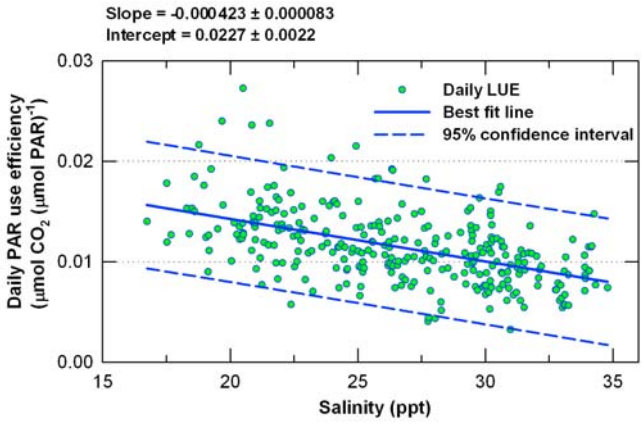

Figure 7. Daily PAR use efficiency (Σ GEP/Σ PAR) when PAR exceeded 600 μmol (photons) m^{-2} s^{-1} as a function of daily average salinity. The regression line and 95% confidence intervals are included.

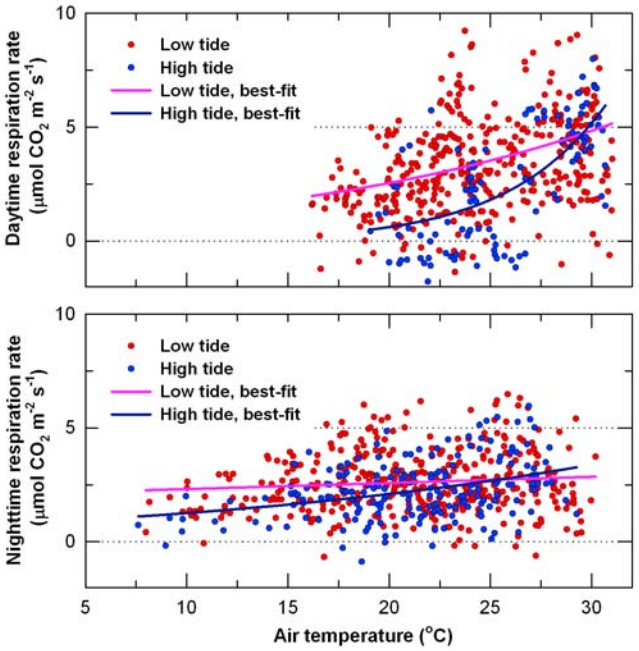

Figure 8. Control of air temperature, measured at 27 m above ground during (top) daytime and (bottom) nighttime, on ecosystem respiration rates determined separately for both low-tide and high-tide periods. Daytime respiration rates represent daily averages, and nighttime respiration rates represent averages during continuous low- or high-tide periods. An Arrhenius-type exponential function was best fit to ecosystem respiration rates during the daytime and nighttime high- and low-tide periods.

3.4. Seasonal and Annual NEP

[24] There were distinctive seasonal patterns in total daily and nighttime NEP (Figure 9). Daily total NEP was greatest between March and May and lower in July through October (Figure 10). During this period, NEP was reduced (NEE of −10 to 0 μmol (CO_2) m^{-2} s^{-1}) during afternoon thunderstorms that reduced solar irradiance (<500 W m^{-2}). However, reductions in NEP values were also observed during cloudless conditions in July to October when the combination of high PAR (>1400 μmol (photons) m^{-2} s^{-1}) and high T_A (>28°C) contributed to increased daytime and nighttime R_d (4–7 μmol (CO_2) m^{-2} s^{-1}). Low NEP (1 to 4 g C m^{-2} d^{-1}) during December to February was attributed to low-temperature inhibition of photosynthesis and shorter day lengths. During December to February reductions in total daily NEP occurred even though this period was also marked by annual minimum respiration rates (1–3 μmol (CO_2) m^{-2} s^{-1}). Low-temperature (T_A < 21°C) effects on carbon assimilation, rather than respiration, caused reduction in NEP during this period.

[25] During 2004, monthly NEP (Figure 10) ranged from 126 ± 9 to 132 ± 15 g C m^{-2} between March and May and varied from 74 ± 10 to 86 ± 8 g C m^{-2} between July and October. NEP increased to 101 ± 10 g C m^{-2} during November as a result of decreasing nighttime temperatures (lower R_d), low salinity stress, and fewer afternoon thunderstorms compared to the warmer summer months. Salinity

Table 3. Mean Daytime and Nighttime Ecosystem Respiration Rates and Arrhenius Model Parameters Under exposed Soil and Inundated Conditions January 2004 Through August 2005[a]

	Daytime		Nighttime	
Summary Characteristic	Exposed Soil at Low Tide	Inundated Soil at High Tide	Exposed Soil at Low Tide	Inundated Soil at High Tide
Number of contiguous periods	398	113	371	191
Mean R_d (μmol m^{-2} s^{-1})	3.48	2.57	2.68	2.20
Mean air temperature (°C)	24.4	25.7	19.6	20.7
$R_{d_{20}}$[b] (μmol m^{-2} s^{-1})	2.546 ± 0.288	0.611 ± 0.298	2.579 ± 0.141	2.101 ± 0.189
E_a/R[b] (K)	5702 ± 1414	18980 ± 4767	899 ± 935	4237 ± 1697
R^2[b]	0.115	0.419	0.011	0.131
RMSE	2.42	2.01	1.33	1.18

[a]Shown with 95% confidence intervals. Exposed soil conditions are at low tide, and inundated conditions are at high tide.
[b]The Arrhenius-type model of *Lloyd and Taylor* [1994] was used to relate ecosystem respiration (R_d) to air temperature T (deg K). $R_d = R_{d20} \exp[(E_a/R)(1/293K - 1/T_K)]$.

values remained low (<29 ppt) during December 2004 to January 2005, but annual minimum NEP values (75 ± 6 to 76 ± 7 g C m^{-2}) during this period were the result of reduced daytime carbon assimilation. During 2004, the mangrove forest assimilated 1170 ± 127 g C m^{-2} (Table 1). During the 8 months of measurements in 2005, the forest assimilated 832 ± 97 g C m^{-2}, which is equivalent to an annual rate of 1175 ± 145 g C m^{-2} yr^{-1}. We found pronounced interannual differences in monthly NEP during 2004 and 2005. For example, NEP in March 2005 was ~20% lower than in March 2004. This resulted from a combination of greater cloud cover, lower solar irradiance, higher nighttime T_A, and higher salinity values during March 2005. In contrast, NEP during July–August 2005 was 35% higher compared to the same period in 2004. The climatic conditions during these months in 2004–2005 were similar, with the exception of local rainfall. At a monitoring station near the tower site, rainfall was 261 mm and 590 mm during June–July 2004 and 2005, respectively. The increased rainfall in 2005 resulted in increased freshwater discharge, which lowered salinity levels, increased the duration of flooding, and lowered soil respiratory fluxes compared to 2004. During June–July 2005, average R_d reached 3.08 ± 1.12 g C m^{-2} s^{-1} whereas in 2004 R_d attained 3.83 ± 1.93 g C m^{-2} s^{-1}.

4. Discussion

[26] Mangrove forest NEP values (1170 ± 145 g C m^{-2}) estimated for 2004–2005 are substantially greater than those reported for terrestrial ecosystems [e.g., *Baldocchi et al.*, 2001; *Luyssaert et al.*, 2007; *Hirata et al.*, 2008]. In general, the annual NEP of tropical ecosystems tends to be greater than that of temperate ecosystems due, in part, to the year-round productivity [*Luyssaert et al.*, 2007]. The high NEP values reported here are reflected in the high leaf litter and wood production, which is reported at 1170 g C m^{-2} yr^{-1} [*Twilley et al.*, 1992]. Relatively low respiration rates (R_d) in the mangrove ecosystem are largely responsible for the high NEP estimates. Nighttime R_d values varied from 1.71 ± 1.44 to 2.84 ± 2.38 μmol (CO_2) m^{-2} s^{-1} at soil temperatures of 15 ± 2°C and 20 ± 2°C, respectively. These R_d values are lower by a factor of 2 compared to terrestrial AmeriFlux and EuroFlux sites whose respiration rates range from 3.72 ± 2.20 to 5.92 ± 4.40 μmol (CO_2) m^{-2} s^{-1} at soil temperatures of 15°C and 20°C, respectively [*Falge et al.*, 2001]. Slow biomass decomposition rates associated with saturated soils and anaerobic conditions result in reduced carbon respiratory losses in mangrove forests [*McKee*, 1993; *Ferreira et al.*, 2007; *Romero et al.*, 2005; *Poret et al.*, 2007].

[27] When integrated over annual periods, the low respiratory fluxes determined at the study site resulted in

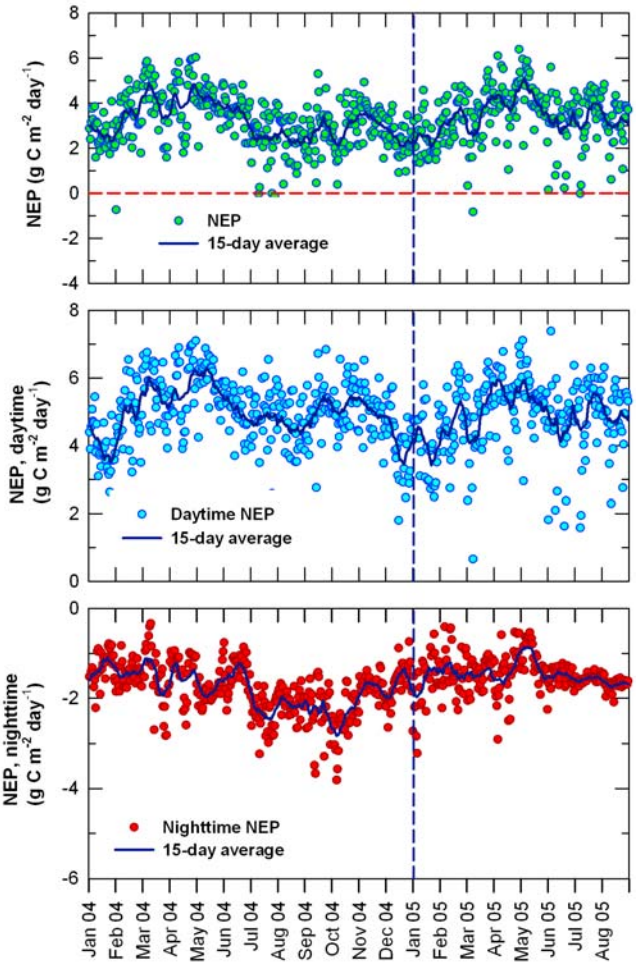

Figure 9. (top) Total daily C NEP and (middle) daytime and (bottom) nighttime contributions to total daily C NEP during January 2004 through August 2005. Centered moving averages (15 day) are included.

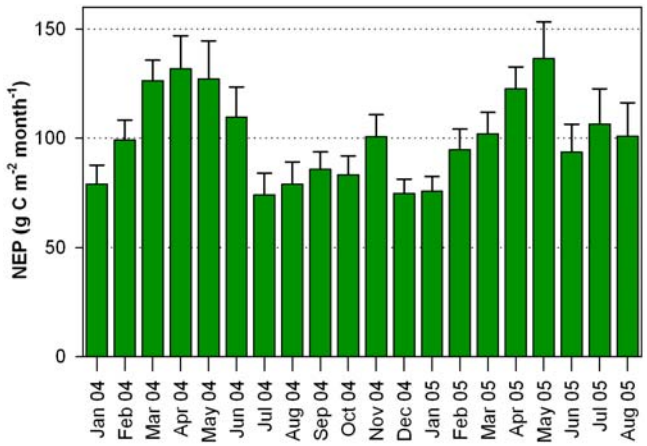

Figure 10. Monthly sums and errors of C NEP during January 2004 through August 2005.

annual ecosystem respiration (R_E) rates during 2004 that were similar to midlatitude terrestrial biomes and significantly lower than other tropical or subtropical evergreen forests (Figure 11). The annual GPP (the sum of NEP and R_E) reported for these tropical systems frequently exceeds 3000 g C m^{-2} [*Kato and Tang*, 2008], with a global average value of 3551 ± 160 g C m^{-2} [*Luyssaert et al.*, 2007]. These GPP values are significantly higher than our estimates in the Florida Everglades mangrove forest. Other tropical and subtropical systems also typically exhibit higher R_E (3061 ± 162 g C m^{-2} [*Luyssaert et al.*, 2007]) compared to our site. As a result, the annual NEP values reported for most other tropical systems are also lower than the present 2004–2005 estimates in the mangrove forest.

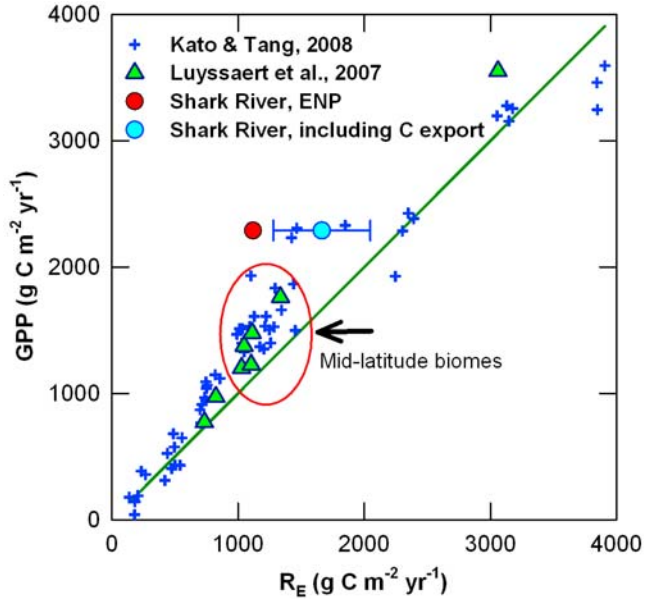

Figure 11. Comparison of mangrove annual GPP and annual R_E with those reported for other ecosystems, where NEP = GPP − R_E.

Table 4. Global Average and Site Level Estimates of Carbon Exports From Tidal Mangrove Forests[a]

	Global Average Value (g C m^{-2} yr^{-1})	Shark River, ENP Value (g C m^{-2} yr^{-1})
Burial	130[b]	130[b]
Particulate organic carbon (POC)	137 ± 172[c]	64[d]–186[e]
Dissolved organic carbon (DOC)	150 ± 134[b]	56[f]
Dissolved inorganic carbon (DIC)	3 × DOC to 10 × DOC[c]	170–560[c,f]
Sum of POC, DOC, and DIC	1262 ± 814	550 ± 260

[a]The global average value of carbon burial was used to estimate the value at Shark River since site-specific values were not available.
[b]*Duarte et al.* [2005].
[c]*Bouillon et al.* [2008].
[d]*Twilley* [1985].
[e]*Heald* [1971].
[f]*Romigh et al.* [2006].

[28] Tidal activity in mangrove forests, such as those found along Shark River, often results in substantial lateral fluxes of particulate and dissolved carbon. This export of carbon will tend to lower estimates of ecosystem respiration derived from EC measurements. For example, benthic microbial decomposition of particulate and dissolved organic carbon (DOC) exported from mangroves [*Souza et al.*, 2009] and from tropical terrestrial forests [*Mayorga et al.*, 2005] results in respiratory fluxes outside of the EC footprint. Similarly, dissolved inorganic carbon (DIC), often found in high concentrations in estuarine waters [*Bouillon et al.*, 2007a; *Miyajima et al.*, 2009] and derived from belowground respiration, is removed by tidal flushing and does not contribute to atmospheric CO_2 fluxes in the forested intertidal zone.

[29] Tidal export of dissolved and particulate organic carbon (POC) from the EC footprint was not measured in 2004–2005. However, the potential magnitude of these fluxes and their influence on our estimates of NEP can be constrained. For example, an extreme upper bound on these fluxes can be estimated as the difference between R_E observed and the R_E values that would be expected in this forest if NEP = 0 (i.e., R_E = −GPP). A forest with NEP = 0 would lie along the 1:1 line in Figure 11. Therefore, the distance along the *x* axis from our observations to this line in Figure 11 represents the difference between R_E and GPP and the potential carbon export assuming NEP = 0 in this system. This provides an upper limit on annual tidal export of ~1000 g C m^{-2} yr^{-1}. However, we consider this an overestimate since this forest is known to accumulate biomass and soil carbon (i.e., NEP ≠ 0). We further constrain the magnitude of tidal carbon export using a combination of direct measurements obtained near our site and a literature review. For example, in a flume study near our site, *Romigh et al.* [2006] estimated a net DOC export rate of 56 g C m^{-2} yr^{-1}. In other mangrove forests along the Everglades Gulf Coast, *Twilley* [1985] and *Heald* [1971] estimated POC exports from 64 to 186 g C m^{-2} yr^{-1}. No direct measurements of DIC fluxes in this region are available. However, in their review of data from other systems, *Bouillon et al.* [2007b, 2008] suggest DIC export can be as much as 3 to 10 times the amount of DOC exported from tidal mangrove forests. Using this relationship between DIC and DOC and the *Romigh*

et al. [2006] estimate of DOC, we estimate the DIC export can be 170 to 560 g C m^{-2} yr^{-1} (Table 4). Therefore, a better estimate of the total dissolved and particulate carbon export from our site is 550 ± 260 g C m^{-2} yr^{-1}.

[30] Adding this estimate of total DOC, DIC, and POC export to the estimates of R_E derived from our NEE measurements yields a GPP/R_E ratio for this forest similar to values reported for other tropical forests [*Kato and Tang*, 2008] (Figure 11). Adding all of the POC and DOC fluxes to R_E may, however, slightly overestimate the influence of these fluxes on NEE since in a system without tidal influences, some fraction of the POC and DOC may not be respired into CO_2 and would instead accumulate in the system. We are unable to quantify the potential bias this introduced into our estimates of tidal carbon export and R_E, but we do not consider this to be a significant term, primarily because the magnitude of POC and DOC fluxes relative to DIC fluxes measured in other mangrove systems is typically small. Estimates of high DIC flux from the mangrove forests at our site are supported by measurements of high partial pressures of carbon dioxide (pCO_2) at the mouth of Shark River [*Clark et al.*, 2004]. We conclude that between 25% and 70% of NEP is exported into the estuary with the remainder accumulating in tree biomass and soil carbon.

[31] There are several important challenges to measuring total carbon export at this site. Commonly applied methods used for determining DOC fluxes on an aerial basis have focused on water-soil surface exchanges across relatively well-defined tidal creeks or man-made flumes. However, high tides often inundate the entire island at our site, and overwash occurs around the island perimeter. The carbon fluxes via this overwash may be significant and will vary over time depending on the amplitude and duration of the tidal cycle. This aspect of the carbon budget at our site requires further examination.

[32] An independent estimate of NEP derived from EC measurements can be calculated as the difference between net primary productivity (NPP), based on biometric data and soil respiration (R_s [*Luyssaert et al.*, 2009]). In tidal systems, the estimates of NEP derived from biometry and R_s do not account for dissolved and particulate carbon export and can therefore be compared directly to our estimates derived from EC. *Bouillon et al.* [2008] suggest an average annual NEP of 1100 ± 644 g C m^{-2} for mangrove ecosystems based on the difference between globally averaged NPP (1363 ± 450 g C m^{-2}) and R_s (263 ± 194 g C m^{-2}). *Komiyama et al.* [2008] provide a similar NEP estimate of 852 g C m^{-2} yr^{-1} for a mangrove forest in eastern Thailand. At our site, *Ewe et al.* [2006] measured aboveground NPP, including increases in basal area and leaf litter, to be 1100 ± 45 g C m^{-2} yr^{-1}. We estimate belowground NPP of 520 ± 360 g C m^{-2} based on a review by *Bouillon et al.* [2008] of results from four studies in southwest Florida close to our site. The locations of these studies share many characteristics with our site and include a fringing forest of *R. mangle*; two mixed species basin forests of *R. mangle*, *L. racemosa*, and *A. germinans*; and an aggregate of sites located in mangrove forests along the east and west coasts of Everglades National Park. Two sets of direct R_S measurements were made at our site in six 20 cm^2 plots using a soil CO_2 flux system (model 8100, LI-COR, Inc., Lincoln, Nebraska). The soil CO_2 efflux rates from these observations ranged between 0.5 to 2.0 μmol m^{-2} s^{-1} (T. Troxler, Florida International University, unpublished data, 2009), and from these data we estimate an annual R_S of 360 ± 180 g C m^{-2} at our site. Subtracting this R_S value from the combined aboveground and belowground NPP values yields a biometric NEP estimate of 1000 ± 400 g C m^{-2}. This value is within the confidence limits of the EC-derived NEP quantities for this ecosystem.

[33] Aboveground respiratory fluxes contributed by foliage, boles, and prop roots are expected to outweigh the belowground components of R_d. During high-tide periods when the soil surface is submerged, the average reductions in R_d from low-tide periods (Figure 8) are roughly equivalent to R_S derived from chamber measurements, which suggest the tides suppress belowground respiratory CO_2 efflux to the atmosphere. There is substantial variability and overlap in R_d across tidal cycles, suggesting temperature effects on aboveground respiratory fluxes throughout the year have a greater effect than tidal influences on R_d. Dark respiration rates in red mangrove foliage are estimated at 1.62 ± 1.32 μmol (CO_2) m^{-2} s^{-1} at 30°C [*Barr et al.*, 2009]. The leaf area index (LAI) at this site in 2008 was measured at 2.29 ± 0.18 (V. Rivera-Monroy, Louisiana State University, personal communication, 2009). Multiplying the foliage dark respiration rate by this estimate of LAI suggests that foliage respiration alone can contribute to 73% of total R_d during low-tide periods. A recent study by *Lovelock* [2008], using data from 10 mangrove forests distributed throughout the Caribbean, Australia, and New Zealand, supports the hypothesis that soil respiration is a relatively minor term in R_d in mangrove forests. For example, applying the *Lovelock* [2008] parabolic relationship between R_S and temperature at the Everglades site yields R_S values of 1.23 and 1.30 μmol (CO_2) m^{-2} s^{-1} at 20°C and 30°C, respectively. These values agree with the direct measurements of soil CO_2 efflux at our site, and represent at most 25 to 41% of nighttime R_d.

[34] Synoptic-scale salinity effects are apparent when relating NEE to PAR and T_A (Figure 6). There is a linear decrease in LUE with increasing salinity across all seasons (Figure 7). Other studies [*Kozlowski*, 1997; *Ball and Farquhar*, 1984; *Sobrado*, 1999; *Parida and Das*, 2005; *Lopez-Hoffman et al.*, 2006] also report negative effects of salinity on mangrove physiological functioning and growth.

[35] Consistent with findings in terrestrial forests [*Gu et al.*, 2002], increases in diffuse solar irradiance (i.e., decreasing K_t) were associated with increasing canopy LUE. However, the positive effects of diffuse solar irradiance were notable only at lower T_A (≤21°C). At higher T_A, high K_t was usually associated with PAR values above the saturation value of 1000 μmol (photons) m^{-2} s^{-1} reported for *R. mangle* [*Barr et al.*, 2009], *Rhizophora mucronata* and *Ceriops tagal* [*Theuri et al.*, 1999], and *Avicennia marina* [*Naidoo et al.*, 1997]. Therefore, a substantial proportion of the mangrove foliage during the summer months can function at or near light saturation conditions, and this process can reduce any positive effects of decreasing K_t on NEE. Leaf orientation is another factor contributing to the lack of K_t effects on NEE during the summer months. Sunlit mangrove foliage orients itself in a more vertical position compared to shaded foliage [*Farnsworth and Ellison*, 1996],

and foliage in the canopy crown can be nearly vertical [*Clough et al.*, 1982]. This adaptation mechanism allows efficient penetration of solar irradiance into deeper regions of the mangrove forest canopy resulting in comparable rates of photosynthesis above and below the forest crown. In the summer months, this strategy can be most effective at dispersing direct beam irradiance throughout the canopy at peak solar elevation angles. During this time, differences in absorption profiles of direct and diffuse solar beam can be small. When solar elevation angles are lower during the dry season months, the penetration of the direct solar beam into deeper regions of the canopy is reduced, and the differences in NEE due to differences in K_t are large (3 to 6 μmol (CO_2) m^{-2} s^{-1}) compared to those (~2 μmol (CO_2) m^{-2} s^{-1}) observed in the summer.

5. Summary and Conclusions

[36] Although much of the variability in the canopy-atmosphere CO_2 exchanges measured above this mangrove forest can be attributed to foliage light and temperature responses, as in terrestrial systems, the influences of tidal activity must be considered when comparing the carbon balance of this system to other forests. During 2004–2005 the annual NEP for this forest was 1170 ± 127 g C m^{-2}. This unusually high NEP is attributed to relatively low respiration rates which are more similar to those of forests growing in temperate climates than to those in tropical zones. We attribute the low R_E to regular tidal inundation and anoxic soil conditions and the net tidal advection of POC, DOC, and DIC from the forest into adjacent estuarine waters. Any potential CO_2 exchanges with the atmosphere derived from the respiration of this exported carbon will occur away from intertidal zones and outside the EC tower footprint. More information on the variability and magnitude of the carbon exports due to tidal activity on daily and seasonal time scales is needed. In addition to tidal influences, salinity effects on mangrove physiological functioning also differentiate carbon cycling in these forests from terrestrial systems. Our results, including the observations of declining LUE with increasing salinity, suggest the long-term carbon balance of this system will largely depend on the factors which control water and salinity levels, such as freshwater discharge from upstream areas, rainfall patterns, and secular sea level rise. These factors are all expected to change with atmospheric warming. These studies are unique because they can help define ecosystem function in response to regional (e.g., freshwater discharge) and global (e.g., sea level rise) environmental change.

[37] **Acknowledgments.** J. G. Barr received support from NASA to carry out the field research outlined in this manuscript and support from the University of Virginia Faculty Senate Dissertation-Year Fellowship to perform data analyses. The National Park Service provided support to carry out the data analyses and interpretation. The National Science Foundation provided support for this research through the Florida Coast Everglades Long-Term Ecological Research program under grants DBI-0620409 and DEB-9910514. The Jones Foundation also provided support for this research. T. J. Smith III and G. H. Anderson were supported by the USGS Terrestrial, Freshwater and Marine Ecosystems and the Global Change Programs. The authors thank James Kathilankal of the AmeriFlux QA/QC group at Oregon State University for his assistance and feedback in verifying output from eddy covariance flux processing software. The authors also thank Caryl Alarcon at Everglades National Park for her assistance with GIS software. Use of trade and product names does not imply endorsement by the U.S. government.

References

Alongi, D. M. (2008), Mangrove forests: Resilience, protection from tsunamis, and responses to global climate change, *Estuarine Coastal Shelf Sci.*, *76*, 1–13, doi:10.1016/j.ecss.2007.08.024.

Baldocchi, D. D. (2008), 'Breathing' of the terrestrial biosphere: Lessons learned from a global network of carbon dioxide flux measurement systems, *Aust. J. Bot.*, *56*, 1–26, doi:10.1071/BT07151.

Baldocchi, D. D., et al. (2001), FLUXNET: A new tool to study the temporal and spatial variability of ecosystem-scale carbon dioxide, water vapor, and energy flux densities, *Bull. Am. Meteorol. Soc.*, *82*, 2415–2434, doi:10.1175/1520-0477(2001)082<2415:FANTTS>2.3.CO;2.

Ball, M. C., and G. D. Farquhar (1984), Photosynthetic and stomatal responses of the grey mangrove, *Avicennia marina*, to transient salinity conditions, *Plant Physiol.*, *74*, 7–11, doi:10.1104/pp.74.1.7.

Ball, M. C., and S. M. Pidsley (1995), Growth responses to salinity in relation to distribution of two mangrove species, *Sonneratia alba* and *S. lanceolata*, in northern Australia, *Funct. Ecol.*, *9*, 77–85, doi:10.2307/2390093.

Barr, J. G. (2005), Carbon sequestration by riverine mangroves in the Florida Everglades, Ph.D. thesis, 183 pp., Univ. of Va., Charlottesville.

Barr, J. G., J. D. Fuentes, V. Engel, and J. C. Zieman (2009), Physiological responses of red mangroves to the climate in the Florida Everglades, *J. Geophys. Res.*, *114*, G02008, doi:10.1029/2008JG000843.

Bouillon, S., F. Dehairs, B. Velimirov, G. Abril, and A. V. Borges (2007a), Dynamics of organic and inorganic carbon across contiguous mangrove and seagrass systems (Gazi Bay, Kenya), *J. Geophys. Res.*, *112*, G02018, doi:10.1029/2006JG000325.

Bouillon, S., J. J. Middleburg, F. Dehairs, A. V. Borges, G. Abril, M. R. Flindt, S. Ulomi, and E. Kristensen (2007b), Importance of intertidal sediment processes and porewater exchange on the water column biogeochemistry in a pristine mangrove creek (Ras Dege, Tanzania), *Biogeosciences*, *4*, 311–322, doi:10.5194/bg-4-311-2007.

Bouillon, S., et al. (2008), Mangrove production and carbon sinks: A revision of global budget estimates, *Global Biogeochem. Cycles*, *22*, GB2013, doi:10.1029/2007GB003052.

Chapman, V. J. (1976), *Mangrove Vegetation*, J. Cramer, Vaduz.

Cheeseman, J. M., and C. E. Lovelock (2004), Photosynthetic characteristics of dwarf and fringe *Rhizophora mangle* L. in a Belizean mangrove, *Plant Cell Environ.*, *27*, 769–780, doi:10.1111/j.1365-3040.2004.01181.x.

Clark, C. D., W. T. Hiscock, F. J. Millero, G. Hitchcock, L. Brand, W. L. Miller, L. Ziolkowski, R. F. Chen, and R. G. Zika (2004), CDOM distribution and CO_2 production on the southwest Florida shelf, *Mar. Chem.*, *89*, 145–167, doi:10.1016/j.marchem.2004.02.011.

Clough, B. F., and R. G. Sim (1989), Changes in gas exchange characteristics and water use efficiency of mangroves in response to salinity and vapour pressure deficit, *Oecologia*, *79*, 38–44, doi:10.1007/BF00378237.

Clough, B. G., T. J. Andrews, and I. R. Cowan (1982), Physiological processes in mangroves, in *Mangrove Ecosystems in Australia: Structure, Function and Management*, edited by B. F. Clough, pp. 193–209, Aust. Natl. Univ. Press, Canberra.

Duarte, C. M., J. J. Middelburg, and N. Caraco (2005), Major role of marine vegetation on the oceanic carbon cycle, *Biogeosciences*, *2*, 1–8, doi:10.5194/bg-2-1-2005.

Duever, M. J., J. F. Meeder, L. C. Meeder, and J. M. McCollom (1994), The climate of south Florida and its role in shaping the Everglades ecosystem, in *Everglades: The Ecosystem and Its Restoration*, edited by S. M. Davis and J. C. Ogden, pp. 225–248, St. Lucie, Delray Beach, Fla.

Ewe, S. M. L., E. E. Gaiser, D. L. Childers, D. Iwaniec, V. H. Rivera-Monroy, and R. R. Twilley (2006), Spatial and temporal patterns of aboveground net primary productivity (ANPP) along two freshwater-estuarine transects in the Florida Coastal Everglades, *Hydrobiologia*, *569*, 459–474, doi:10.1007/s10750-006-0149-5.

Falge, E., et al. (2001), Gap filling strategies for defensible annual sums of net ecosystem exchange, *Agric. For. Meteorol.*, *107*, 43–69, doi:10.1016/S0168-1923(00)00225-2.

Farnsworth, E. J., and A. M. Ellison (1996), Sun-shade adaptability of the red mangrove, *Rhizophora mangle* (*Rhizophoraceae*): Changes through ontogeny at several levels of biological organization, *Am. J. Bot.*, *83*, 1131–1143, doi:10.2307/2446196.

Feller, I. C., D. F. Whigham, K. L. McKee, and C. E. Lovelock (2003), Nitrogen limitation of growth and nutrient dynamics in a disturbed mangrove forest, *Indian River Lagoon, Florida, Oecologia*, *134*, 405–414.

Ferreira, T. O., X. L. Otero, P. Vidal-Torrado, and F. Macias (2007), Redox processes in mangrove soils under *Rhizophora mangle* in relation to different environmental conditions, *Soil Sci. Soc. Am. J.*, *71*(2), 484–491.

Goulden, M. L., J. W. Munger, S. M. Fan, B. C. Daube, and S. C. Wofsy (1996), Exchange of carbon dioxide by a deciduous forest: Response to interannual climate variability, *Science*, *271*, 1576–1578, doi:10.1126/science.271.5255.1576.

Gu, L., D. D. Baldocchi, S. B. Verma, T. A. Black, T. Vesala, E. M. Falge, and R. R. Dowty (2002), Advantages of diffuse radiation for terrestrial ecosystem productivity, *J. Geophys. Res.*, *107*(D6), 4050, doi:10.1029/2001JD001242.

Gu, L., et al. (2005), Objective threshold determination for nighttime eddy flux filtering, *Agric. For. Meteorol.*, *128*, 179–197, doi:10.1016/j.agrformet.2004.11.006.

Heald, E. (1971), The production of organic detritus in a south Florida estuary, *Sea Grant Tech. Bull.*, *6*, 110 pp., Univ. of Miami, Miami, Fla.

Hirata, R., et al. (2008), Spatial distribution of carbon balance in forest ecosystems across East Asia, *Agric. For. Meteorol.*, *148*, 761–775, doi:10.1016/j.agrformet.2007.11.016.

Humphreys, E. R., T. A. Black, K. Morgenstern, Z. Li, and Z. Nesic (2005), Net ecosystem production of a Douglas-fir stand for 3 years following clearcut harvesting, *Global Change Biol.*, *11*, 450–464, doi:10.1111/j.1365-2486.2005.00914.x.

Kato, T., and Y. Tang (2008), Spatial variability and major controlling factors of CO_2 sink strength in Asian terrestrial ecosystems: Evidence from eddy covariance data, *Global Change Biol.*, *14*, 2333–2348, doi:10.1111/j.1365-2486.2008.01646.x.

Koch, M. S. (1997), *Rhizophora mangle L.* seedling development into the sapling stage across resource and stress gradients in subtropical Florida, *Biotropica*, *29*, 427–439, doi:10.1111/j.1744-7429.1997.tb00037.x.

Komiyama, A., J. E. Ong, and S. Poungparn (2008), Allometry, biomass, and productivity of mangrove forests: A review, *Aquat. Bot.*, *89*, 128–137, doi:10.1016/j.aquabot.2007.12.006.

Kozlowski, T. T. (1997), Responses of woody plants to flooding and salinity, *Tree Physiol. Online Monogr.*, *1*, 29 pp., Heron, Victoria, B. C., Canada.

Krauss, K. W., J. A. Allen, and D. R. Cahoon (2003), Differential rates of vertical accretion and elevation change among aerial root types in Micronesian mangrove forests, *Estuarine Coastal Shelf Sci.*, *56*, 251–259, doi:10.1016/S0272-7714(02)00184-1.

Krauss, K. W., T. W. Doyle, R. R. Twilley, V. H. Rivera-Monroy, and J. K. Sullivan (2006), Evaluating the relative contributions of hydroperiod and soil fertility on growth of south Florida mangroves, *Hydrobiologia*, *569*, 311–324, doi:10.1007/s10750-006-0139-7.

Lee, X., J. D. Fuentes, R. M. Staebler, and H. H. Neumann (1999), Long-term observation of the atmospheric exchange of CO_2 with a temperate deciduous forest in southern Ontario, Canada, *J. Geophys. Res.*, *104*, 15,975–15,984, doi:10.1029/1999JD900227.

Lloyd, J., and J. A. Taylor (1994), On the temperature dependence of soil respiration, *Funct. Ecol. 8*, 315–323, doi:10.2307/2389824.

Lopez-Hoffman, L., J. L. DeNoyer, I. E. Monroe, R. Shaftel, N. P. R. Anten, M. Martinez-Ramos, and D. D. Ackerly (2006), Mangrove seedling net photosynthesis, growth, and survivorship are interactively affected by salinity and light, *Biotropica*, *38*(5), 606–616, doi:10.1111/j.1744-7429.2006.00189.x.

Lovelock, C. E. (2008), Soil respiration and belowground carbon allocation in mangrove forests, *Ecosystems*, *11*, 342–354, doi:10.1007/s10021-008-9125-4.

Lovelock, C. E., I. C. Feller, K. L. McKee, B. M. J. Engelbrecht, and M. C. Ball (2004), The effect of nutrient enrichment on growth, photosynthesis and hydraulic conductance of dwarf mangroves in Panama, *Funct. Ecol.*, *18*, 25–33, doi:10.1046/j.0269-8463.2004.00805.x.

Lovelock, C. E., M. C. Ball, B. Choat, B. M. J. Engelbrecht, N. M. Holbrook, and I. C. Feller (2006), Linking physiological processes with mangrove forest structure: Phosphorus deficiency limits canopy development, hydraulic conductivity and photosynthetic carbon gain in dwarf *Rhizophora mangle*, *Plant Cell Environ.*, *29*, 793–802, doi:10.1111/j.1365-3040.2005.01446.x.

Luyssaert, S., et al. (2007), CO_2 balance of boreal, temperate, and tropical forests derived from a global database, *Global Change Biol.*, *13*, 2509–2537, doi:10.1111/j.1365-2486.2007.01439.x.

Luyssaert, S., et al. (2009), Toward a consistency cross-check of eddy covariance flux-based and biometric estimates of ecosystem carbon balance, *Global Biogeochem. Cycles*, *23*, GB3009, doi:10.1029/2008GB003377.

Mayorga, E., A. K. Aufdenkampe, C. A. Masiello, A. V. Krusche, J. I. Hedges, P. D. Quay, J. E. Richey, and T. A. Brown (2005), Young organic matter as a source of carbon dioxide outgassing from Amazonian rivers, *Nature*, *436*, 538–541, doi:10.1038/nature03880.

McKee, K. L. (1993), Soil physiochemical patterns and mangrove species distribution-Reciprocal effects?, *J. Ecol.*, *81*, 477–487, doi:10.2307/2261526.

Mitsch, W. J., and J. G. Gosselink (2000), The value of wetlands: Importance of scale and landscape setting, *Ecol. Econ.*, *35*, 25–33, doi:10.1016/S0921-8009(00)00165-8.

Miyajima, T., Y. Tsuboi, Y. Tanaka, and I. Koike (2009), Export of inorganic carbon from two Southeast Asian mangrove forests to adjacent estuaries as estimated by the stable isotope composition of dissolved inorganic carbon, *J. Geophys. Res.*, *114*, G01024, doi:10.1029/2008JG000861.

Moffat, A. M., et al. (2007), Comprehensive comparison of gap-filling techniques for eddy covariance net carbon fluxes, *Agric. For. Meteorol.*, *147*, 209–232, doi:10.1016/j.agrformet.2007.08.011.

Morgenstern, K., T. A. Black, E. R. Humphreys, T. J. Griffis, G. B. Drewitt, T. Cai, Z. Nesic, D. L. Spittlehouse, and N. J. Livingston (2004), Sensitivity and uncertainty of the carbon balance of a Pacific Northwest Douglas-fir forest during an El Nino/La Nina cycle, *Agric. For. Meteorol.*, *123*, 201–219, doi:10.1016/j.agrformet.2003.12.003.

Naidoo, G., H. Rogalla, and D. J. von Willert (1997), Gas exchange responses of mangrove species, *Avicennia marina*, to waterlogged and drained conditions, *Hydrobiologia*, *352*, 39–47 doi:10.1023/A:1003088803335.

Parida, A. K., and A. B. Das (2005), Salt tolerance and salinity effects on plants: A review, *Ecotoxicol. Environ. Safety*, *60*, 324–349, doi:10.1016/j.ecoenv.2004.06.010.

Parida, A. K., A. B. Das, and B. Mittra (2004), Effects of salt on growth, ion accumulation, photosynthesis and leaf anatomy of the mangrove, *Bruguierra parviflora*, *Trees*, *18*, 167–174, doi:10.1007/s00468-003-0293-8.

Poret, N., R. R. Twilley, V. H. Rivera-Monroy, and C. Coronada-Molina (2007), Belowground decomposition of mangrove roots in Florida Coastal Everglades, *Estuaries Coasts*, *30*(3), 491–496, doi:10.1007/BF02819395.

Robertson, A. I., and D. M. Alongi (Eds.) (1992), *Tropical Mangrove Ecosystems, Coastal and Estuarine Sci.*, vol. 41, 329 pp., AGU, Washington, D. C.

Romero, L. M., T. J. Smith III, and J. W. Fourqurean (2005), Changes in mass and nutrient content of wood during decomposition in a south Florida mangrove forest, *J. Ecol.*, *93*, 618–631, doi:10.1111/j.1365-2745.2005.00970.x.

Romigh, M. M., S. E. Davis III, V. H. Rivera-Monroy, and R. R. Twilley (2006), Flux of organic carbon in a riverine mangrove wetland in the Florida Coastal Everglades, *Hydrobiologia*, *569*, 505–516, doi:10.1007/s10750-006-0152-x.

Schmid, H. P. (2002), Footprint modeling for vegetation atmosphere exchange studies: A review and perspective, *Agric. For. Meteorol.*, *113*, 159–183, doi:10.1016/S0168-1923(02)00107-7.

Schotanus, P., F. T. M. Nieuwstadt, and H. A. R. De Bruin (1983), Temperature measurement with a sonic anemometer and its application to heat and moisture fluctuations, *Boundary Layer Meteorol.*, *26*, 81–93, doi:10.1007/BF00164332.

Schuepp, P. H., M. Y. LeClerc, J. I. MacPherson, and R. L. Desjardins (1990), Footprint prediction of scalar fluxes from analytical solutions of the diffusion equation, *Boundary Layer Meteorol.*, *50*, 355–373, doi:10.1007/BF00120530.

Smith, T. J., III, M. B. Robblee, H. R. Wanless, and T. W. Doyle (1994), Mangroves, hurricanes, and lightning strikes, *BioScience*, *44*(4), 256–262, doi:10.2307/1312230.

Sobrado, M. A. (1999), Leaf photosynthesis of the mangrove *Avicennia germinans* as affected by NaCl, *Photosynthetica*, *36*(4), 547–555, doi:10.1023/A:1007092004582.

Souza, M. F. L., V. R. Gomes, S. S. Freitas, R. C. B. Andrade, and B. Knoppers (2009), Net ecosystem metabolism and nonconservative fluxes of organic matter in a tropical mangrove estuary, Piaui River (NE of Brazil), *Estuaries Coasts*, *32*, 111–122, doi:10.1007/s12237-008-9104-1.

Spackman, W., C. P. Dolsen, and W. Riegel (1966), Phytogenic organic sediments and sedimentary environments in the Everglades-mangrove complex. Part I—Evidence of a transgressing sea and its effect on environments of the Shark River area of southwest Florida, *Palaeontographica B, 17*, 135–152.

Spitters, C. J. T., H. A. J. M. Tussaint, and J. Goudriaan (1986), Separating the diffuse and direct component of global radiation and its implications for modeling canopy photosynthesis, part I. Components of incoming radiation, *Agric. For. Meteorol.*, *38*, 217–229, doi:10.1016/0168-1923(86)90060-2.

Stumpf, R. P., and J. W. Haines (1998), Variations in tidal level in the Gulf of Mexico and implications for tidal wetlands, *Estuarine Coastal Shelf Sci.*, *46*, 165–173, doi:10.1006/ecss.1997.0276.

Suárez, N., and E. Medina (2006), Influence of salinity on Na^+ and K^+ accumulation, and gas exchange in *Avicennia germinans*, *Photosynthetica*, *44*, 268–274, doi:10.1007/s11099-006-0018-5.

Takemura, T., N. Hanagata, K. Sugihara, S. Baba, I. Karube, and Z. Dubinsky (2000), Physiological and biochemical responses to salt stress in the mangrove, *Bruguierra gymnorrhiza, Aquat. Bot.*, *68*, 15–28, doi:10.1016/S0304-3770(00)00106-6.

Theuri, M. M., J. I. Kinymario, and D. V. Speybroeck (1999), Photosynthesis and related physiological processes in two mangrove species, *Rhizophora mucronata* and *Ceriops tagal*, at Gazi Bay, Kenya, *Afr. J. Ecol.*, *37*, 180–193, doi:10.1046/j.1365-2028.1999.00167.x.

Tomlinson, P. B. (1986), *The Botany of Mangroves*, Cambridge Univ. Press, Cambridge, U. K.

Twilley, R. R. (1985), The exchange of organic carbon in basin mangrove forests in a southwest Florida estuary, *Estuarine Coastal Shelf Sci.*, *20*, 543–557, doi:10.1016/0272-7714(85)90106-4.

Twilley, R. R., R. H. Chen, and T. Hargis (1992), Carbon sinks in mangrove forests and their implications to the carbon budget of tropical coastal ecosystems, *Water Air Soil Pollut.*, *64*, 265–288, doi:10.1007/BF00477106.

Vickers, D., and L. Mahrt (1997), Quality control and flux sampling problems for tower and aircraft data, *J. Atmos. Oceanic Technol.*, *14*(3), 512–526, doi:10.1175/1520-0426(1997)014<0512:QCAFSP>2.0.CO;2.

Ward, G. A., T. J. Smith III, K. R. T. Whelan, and T. W. Doyle (2006), Regional processes in mangrove ecosystems: Spatial scaling relationships, biomass, and turnover rates following catastrophic disturbance, *Hydrobiologia*, *569*, 517–527, doi:10.1007/s10750-006-0153-9.

Webb, E. K., G. I. Pearman, and R. Leuning (1980), Correction of the flux measurements for density effects due to heat and water vapor transfer, *Q. J. R. Meteorol. Soc.*, *106*, 85–100, doi:10.1002/qj.49710644707.

Whelan, K. R. T., T. J. Smith III, D. R. Cahoon, J. C. Lynch, and G. H. Anderson (2005), Groundwater control of mangrove surface elevation: Shrink and swell varies with soil depth, *Estuaries*, *28*(6), 833–843, doi:10.1007/BF02696013.

Wofsy, S. C., and R. C. Harris (2002), The North American carbon program (NACP), report of the NACP Committee of the U.S. Interagency Carbon Cycle Science Program, 56 pp., U.S. Global Change Res. Program, Washington, D. C.

G. H. Anderson, Everglades National Park Field Station, Florida Integrated Science Center, U.S. Geological Survey, 40001 State Rd. 9336, Homestead, FL 33034, USA.

J. G. Barr and V. Engel, South Florida Natural Resource Center, Everglades National Park, Homestead, FL 33204, USA. (jordanbarr@nps.gov)

J. D. Fuentes, Department of Meteorology, Pennsylvania State University, University Park, PA 16802, USA.

T. L. O'Halloran, Department of Forest Ecosystems and Society, Oregon State University, Corvallis, OR 97331, USA.

T. J. Smith III, Florida Integrated Science Center, U.S. Geological Survey, 600 Fourth St. S., St. Petersburg, FL 33701, USA.

J. C. Zieman, Department of Environmental Sciences, University of Virginia, Charlottesville, VA 22904, USA.